JACS
JOURNAL OF THE AMERICAN CHEMICAL SOCIETY
pubs.acs.org/JACS
Article

Noncryogenic Air Separation Using Aluminum Formate $Al(HCOO)_3$ (ALF)

Dinesh Mullangi,[○] Hayden A. Evans,*[,○] Taner Yildirim, Yuxiang Wang, Zeyu Deng, Zhaoqiang Zhang, Thuc T. Mai, Fengxia Wei, John Wang, Angela R. Hight Walker, Craig M. Brown, Dan Zhao,* Pieremanuele Canepa,* and Anthony K. Cheetham*

Cite This: https://doi.org/10.1021/jacs.3c02100

Read Online

ACCESS | Metrics & More | Article Recommendations | Supporting Information

ABSTRACT: Separating oxygen from air to create oxygen-enriched gas streams is a process that is significant in both industrial and medical fields. However, the prominent technologies for creating oxygen-enriched gas streams are both energy and infrastructure intensive as they use cryogenic temperatures or materials that adsorb N_2 from air. The latter method is less efficient than the methods that adsorb O_2 directly. Herein, we show, via a combination of gas adsorption isotherms, gas breakthrough experiments, neutron and synchrotron X-ray powder diffraction, Raman spectroscopy, and computational studies, that the metal−organic framework, $Al(HCOO)_3$ (ALF), which is easily prepared at low cost from commodity chemicals, exhibits substantial O_2 adsorption and excellent time-dependent O_2/N_2 selectivity in a range of 50−125 near dry ice/solvent (≈190 K) temperatures. The effective O_2 adsorption with ALF at ≈190 K and ≈0.21 bar (the partial pressure of O_2 in air) is ≈1.7 mmol/g, and at ice/salt temperatures (≈250 K), it is ≈0.3 mmol/g. Though the kinetics for full adsorption of O_2 near 190 K are slower than at temperatures nearer 250 K, the kinetics for initial O_2 adsorption are fast, suggesting that O_2 separation using ALF with rapid temperature swings at ambient pressures is a potentially viable choice for low-cost air separation applications. We also present synthetic strategies for improving the kinetics of this family of compounds, namely, via Al/Fe solid solutions. To the best of our knowledge, ALF has the highest O_2/N_2 sorption selectivity among MOF adsorbents without open metal sites as verified by co-adsorption experiments..

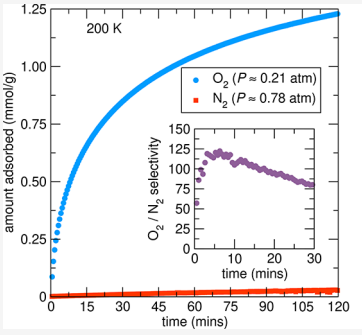

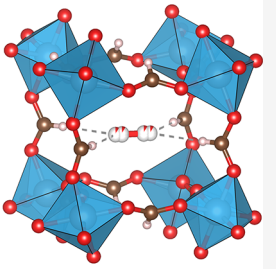

INTRODUCTION

Production of oxygen from air is an important commercial process with upward of 50 billion dollars in global market value annually. O_2 gas is widely used in numerous applications, ranging from its large-scale use in steel production[1] to medical uses for the treatment of people with breathing problems and other conditions.[2] These different applications require O_2 with various levels of purity, ranging from 90% to greater than 99%. During the COVID-19 pandemic, demand for medical O_2 has increased dramatically since it is used to treat COVID-19 patients with breathing difficulties. Unfortunately, in many parts of the globe where the O_2 purification infrastructure is limited and COVID-19 caseloads are high, the demand for medical oxygen has created situations where those in need of treatment are unable to get it. In these circumstances, low-cost O_2 purification technologies are highly desirable as they provide a timely strategy for mitigating such shortages.

On a commercial scale, air separation is usually achieved either through the cryogenic (<120 K) distillation of liquid air,[3] since oxygen boils at 90 K and nitrogen at 77 K, or by the preferential adsorption of N_2 from dry air using lithium-containing zeolites in a pressure swing adsorption process at ambient temperatures.[4,5] Pressure swing adsorption with carbon molecular sieves (CMS) has also been employed for air separation, given the faster oxygen diffusion into CMS than N_2.[6] There are also membrane technologies based on polymers[7] and ceramics,[8] though the former have modest selectivity and the latter require elevated temperatures. In the last decade, there has been a significant effort to develop metal−organic frameworks (MOFs) as selective sorbents for the capture, storage, and release of oxygen.[9] There are two primary strategies involving different adsorption mechanisms. First, there are MOFs that adsorb oxygen via a redox mechanism involving the binding of O_2 to open metal sites or bridging ligands,[10,11] and second, there are size-selective MOFs that adsorb O_2 in preference to the larger N_2 molecule.[12,13] The former approach is challenging because

Received: February 26, 2023

Downloaded via NATL UNIV OF SINGAPORE on April 22, 2023 at 02:12:20 (UTC).
See https://pubs.acs.org/sharingguidelines for options on how to legitimately share published articles.

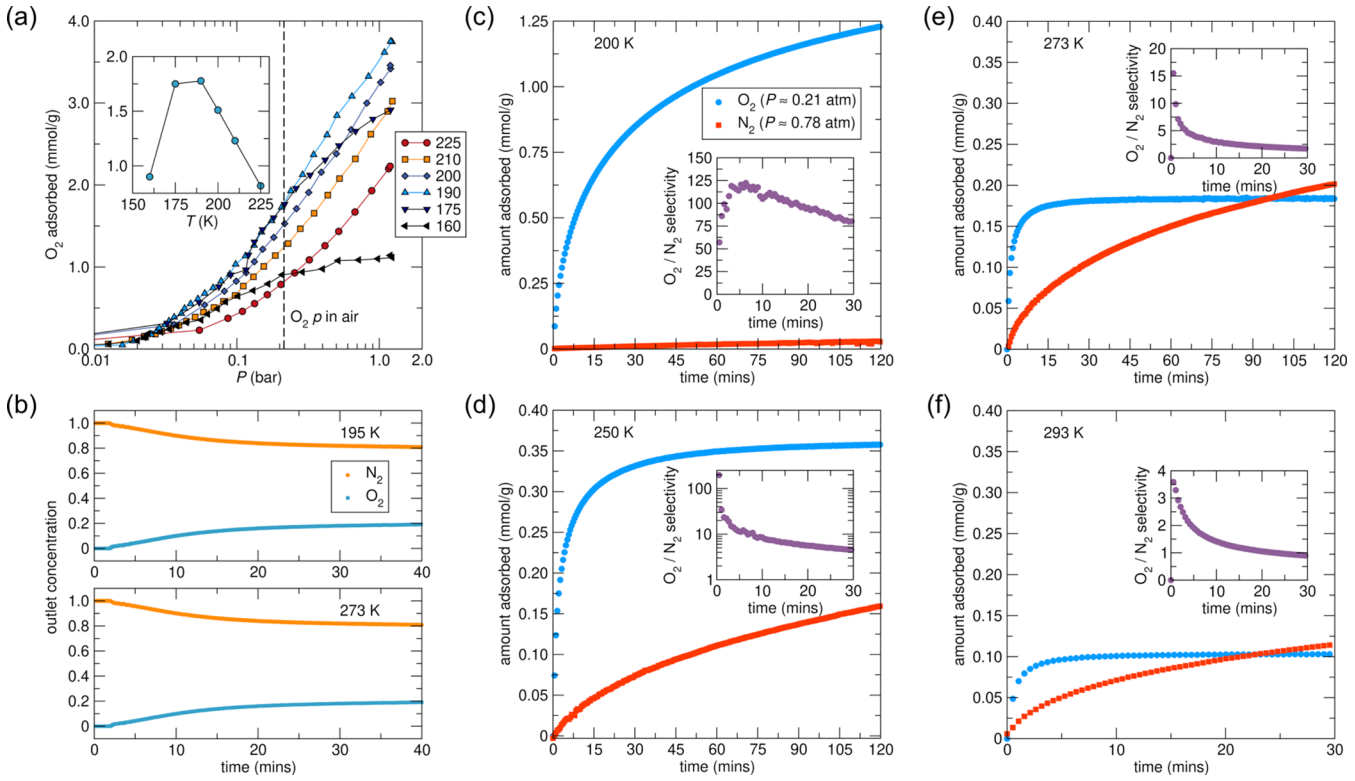

Figure 1. (a) O_2 adsorption isotherms of ALF. The inset graph shows the values for O_2 adsorption versus temperature at the partial pressure of O_2 in air (≈0.21 bar, dashed line in main figure panel). The *y*-axis units are the same as the larger graph. As shown in Figure S9, increased adsorption occurs at temperatures below 250 K, but the hysteresis at these temperatures for O_2 adsorption/desorption grows more pronounced. (b) (Top and bottom) Breakthrough curves of N_2 and O_2 in breakthrough experiments of 21/79 O_2/N_2 mixtures through the ALF packed bed at (top) 195 K and (bottom) 273 K. (c–f) ALF O_2/N_2 adsorption profiles (kinetic curves) at 200, 250, 273, and 293 K. The pressures of O_2 and N_2 are ≈0.21 and ≈0.78 atm, respectively. Time-dependent ideal selectivity calculated from the corresponding O_2 and N_2 uptake is shown in inset graphs for each temperature (violet circles). Figure legend from panel (c) applies to panels (c)–(f).

the binding of O_2 is often quite strong and O_2 release can be difficult. The second strategy is also challenging, as the O_2 and N_2 molecules are very similar in size (kinetic diameters: 346 and 364 pm, respectively). More recent studies in this area include an evaluation of MOFs for O_2 capture using grand canonical Monte Carlo simulations, which predicted and validated excellent performance by HKUST-1 and NU-125,[14] and a novel Al-soc-MOF-1 framework that outperforms even these materials.[15]

Given the challenges of O_2/N_2 separation, materials that have selectivities upward of 5 are considered effective. For example, the commercially utilized Li-containing zeolites,[16] which adsorb N_2 over O_2 at room temperature, have selectivities between 3 and 9, and any material that demonstrates selectivities greater than 10 above cryogenic temperatures is considered excellent. Examples of materials that adsorb O_2 preferentially include the MOFs Fe-MOF-74,[17] which shows an O_2/N_2 selectivity of ≈10 at 226 K, Co-BDTriP, which has an O_2/N_2 selectivity of ≈100 at 195 K,[18] and $Cr_3(BTC)_2$, with an O_2/N_2 selectivity of ≈20 at 298 K.[19] The aforementioned selectivities were derived from isotherm values for dried O_2 and N_2 at 0.21 and 0.78 bar, respectively, which correspond to the partial pressures of these gases in 1 bar of air. However, each of these materials has drawbacks; $Cr_3(BTC)_2$ undergoes material degradation with unregulated O_2 adsorption, while Co-BDTriP requires complex and expensive ligands. In fact, most MOFs are too expensive for commercial adoption compared with zeolites.

The recent review by Hill and co-workers[9] emphasized several desirable requirements for MOFs that could be used for air separation, including (i) reversible sorption without collapse of the MOF structure and (ii) a composition that is suitable for large-scale production at low cost. In this context, we recently reported an earth-abundant, scalable, and highly selective MOF material for CO_2 capture.[20] Aluminum formate, $Al(HCOO)_3$ (ALF), which has an ReO_3-type structure[21] is capable of adsorbing CO_2 from CO_2-rich flue gas streams with high CO_2/N_2 selectivity. As discussed in our previous study,[20] the structure of ALF contains two types of cavities, small and large, which are differentiated by how the hydrogens of the formates point toward or away from the center of each cavity, respectively. The small cavity favors CO_2 adsorption relative to the large cavity because the hydrogen bonding from the formate hydrogens facilitates a "hand-in-glove" relationship with CO_2. Remarkably, ALF excludes N_2 from its cavities at most temperatures despite the very similar kinetic diameters of CO_2 and N_2 (330 and 364 pm, respectively). Based on these previous results, we hypothesized that O_2 (kinetic diameter 346 pm), with its smaller size compared with N_2, could also access the cavities of ALF. In the present work, we confirm our hypothesis and demonstrate that the affordable and easily prepared metal–organic framework ALF, and its related Al/Fe solid solutions, denoted here as ALF-Fe, exhibit excellent O_2 adsorption and O_2/N_2 selectivity at sub 1 bar pressures in a temperature range of 190–250 K.

https://doi.org/10.1021/jacs.3c02100
J. Am. Chem. Soc. XXXX, XXX, XXX–XXX

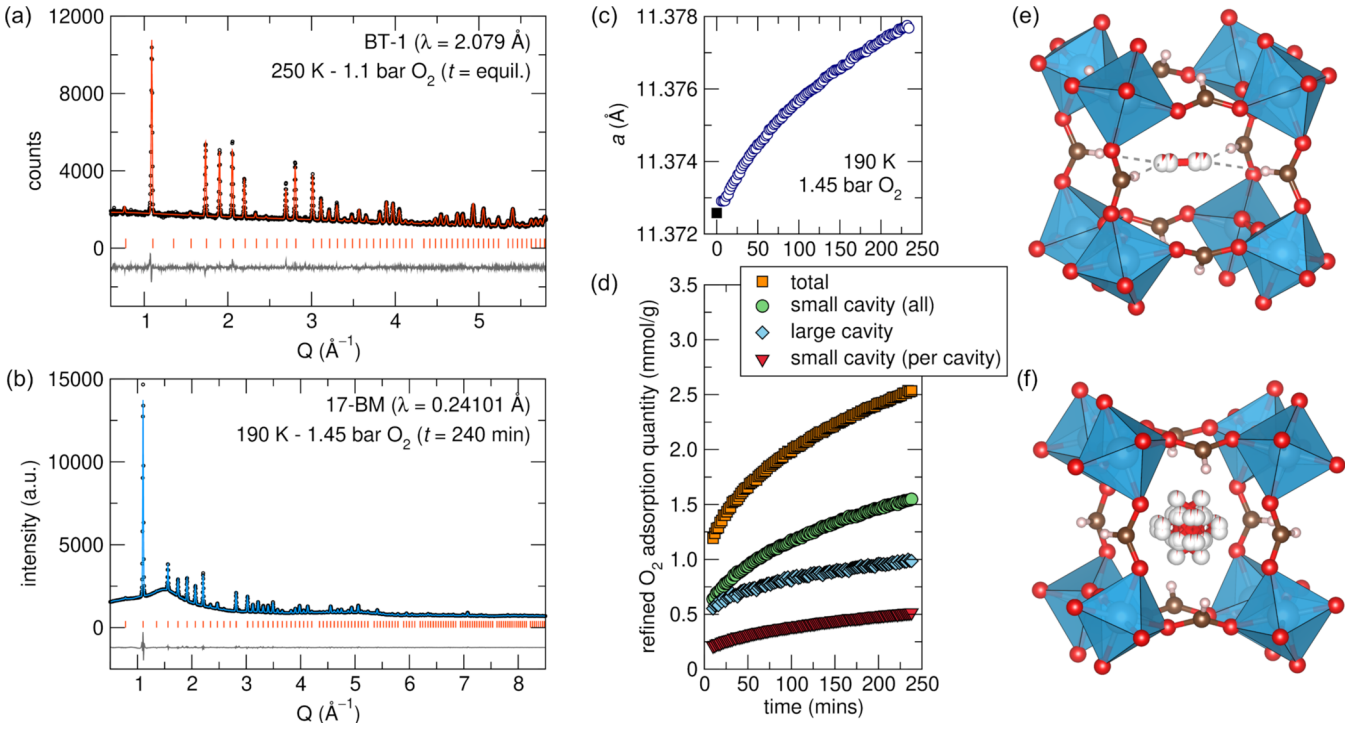

Figure 2. Rietveld refinement results of in situ neutron and synchrotron X-ray diffraction experiments of ALF under constant O_2 pressures. (a) Rietveld fit of the neutron dataset of ALF under 1.1 bar O_2 at 250 K after 6 h of equilibration. [NCNR, BT-1, λ = 2.079 Å] SG = $Im\bar{3}$, a = 11.3808(1) Å, R_{wp} = 2.81%, R_p = 2.24%. Black circles = data, red line = fit, red ticks = predicted *hkl*s, and gray line = difference. (b) Representative fit of synchrotron X-ray diffraction data [APS, 17-BM, λ = 0.24101 Å] at 190 K under 1.45 bar O_2. Shown data is for the 240 min dataset. SG = $Im\bar{3}$, a = 11.3811(1) Å, R_{wp} = 2.24%, R_p = 1.40%. Black circles = data, blue line = fit, red ticks = predicted *hkl*s, and gray line = difference. (c) and (d) Results from sequential Rietveld refinements of 17-BM data, where ALF was exposed to 1.45 bar of O_2 at 190 K and monitored over the course of 240 min. Data point sizes are commensurate with error bars (1σ). (c) Change in the unit cell parameter a as a function of time of ALF under 1.45 bar O_2 between 0 and 240 min. Black square denotes unit cell value of activated structure at 190 K. (d) Refined O_2 occupancy normalized to mmol/g over the course of the experiment. There are 3 times as many small cavities as large cavities in the crystal structure. The red trace shows the mmol/g for one small cavity and serves as a direct comparison between the large cavity mmol/g adsorption. Errors were propagated for the combined total. (e) Structural depiction of the small cavity of ALF filled with O_2 from the Rietveld refinement results from the 240 min dataset. The structure shows how, within the small cavity of ALF, hydrogen bonding exists between the formate hydrogens and O_2 molecules. There is one oxygen per small cavity, but the disordered molecules illustrate how the oxygen may prefer one side of the cavity or the other. The distances between the H of the formate ligand and each O of the O_2 molecule are 2.82(9) and 2.99(9) Å. (f) Structural depiction of the large cavity of ALF with a disordered O_2 molecule inside. There is one oxygen per large cavity, with the disorder denoting the many possible positions it may take. There is no hydrogen bonding present in the large cavity. Representative refinement fits from the sequential fitting, as well as specific details of the refinements, and all results can be found in the Supporting Information.

RESULTS AND DISCUSSION

Adsorption and desorption O_2 isotherms with ALF were measured in the temperature range of 125−298 K, where Figure 1a shows selected adsorption isotherms (Figure S9 shows both adsorption\desorption curves). ALF displays effective peak O_2 adsorption at pressures between 0 and 1.2 bar at 190 K, with ≈3.5 mmol/g being adsorbed at 1.2 bar. At ≈0.21 bar (the partial pressure of O_2 in air), effective peak O_2 adsorption with ALF is also seen near 190 K with adsorption of ≈1.5 mmol/g. This notable noncryogenic temperature O_2 adsorption is even more impressive when coupled with ALF high O_2/N_2 selectivity at 200 K, which is illustrated in Figure 1c. Figure 1b shows the air separation performance of ALF at 195 and 273 K probed using dynamic breakthrough experiments with simulated dry air containing 21% O_2 with N_2 as the balance. As shown, N_2 broke through the column before O_2, suggesting that ALF preferentially adsorbs O_2 over N_2 under co-adsorption conditions at 195 K. Quantitative analyses of the breakthrough curves show a pseudo-equilibrium O_2 uptake of 0.66 mmol/g at 195 K. During this breakthrough experiment, the N_2 uptake in ALF was so low that no uptake capacity could be determined in either the adsorption or desorption runs of the breakthrough experiments. This very low adsorption of N_2 at 195 K is consistent with our more detailed kinetic isotherm experiments conducted at 200 K, which show that ALF slowly adsorbs N_2 but at amounts of ≈0.05 mmol/g over 2 h (Figure 1c). Furthermore, the separation performances can be maintained, even if the particle size varies (Figure S20). These results indicate that the cavities of ALF are mostly inaccessible to N_2 and that the lower calculated O_2 uptake from breakthrough experiments, when compared to isotherm values, may result from unestablished sorption equilibrium within the time frame of the breakthrough experiment. As shown in Figure 1e, when the temperature was increased to ≈273 K, dynamic O_2 uptake in ALF was reduced to ≈0.2 mmol/g and ALF did not effectively separate O_2 from N_2, as indicated by the reduced area between O_2 and N_2 breakthrough curves. This is further shown in Figure 1e, where at 273 K, initial O_2 adsorption is fast but plateaus quickly. Selectivity is initially ≈10 but drops to near unity after 30 min. This drop in selectivity is contrasted by the O_2/N_2 adsorption behavior at 200 K, where ALF displays an O_2/N_2 selectivity of

https://doi.org/10.1021/jacs.3c02100
J. Am. Chem. Soc. XXXX, XXX, XXX−XXX

≈125 within 5 min of adsorption that slowly decreases to ≈75 after 30 min as O_2 adsorption begins to plateau. Given that ALF has moderate sensitivity to moisture at temperatures above 311 K,[20] the sub-273 K O_2 adsorption temperatures would account for a drying step in practical use. In addition, CO_2 adsorption from air into ALF is known to be extremely low.[20]

To observe the behavior of ALF at the atomic level upon O_2 adsorption, in situ neutron and synchrotron X-ray diffraction experiments were conducted, and the results are shown in Figure 2. Figure 2a shows the powder neutron diffraction Rietveld refinement of ALF at 250 K and 1.1 bar of O_2, and Figure 2b–d shows the results of real-time in situ monitoring via synchrotron X-ray diffraction of ALF at 190 K and 1.45 bar O_2. Though both experiments provide information about how the crystal structure of ALF fills with O_2, the synchrotron X-ray diffraction experiment provided real-time monitoring via rapid acquisition alongside simultaneous Raman spectroscopy (discussed below). Figure 2b shows a representative fit of an X-ray dataset of ALF at 190 K and a 1.45 bar (1100 Torr) O_2 atmosphere. The specific dataset shown was collected after 240 min of O_2 exposure. Figure 2c shows how, over the course of 240 min under 1.45 bar of O_2, the lattice parameter of ALF increases slightly as O_2 is adsorbed. This contrasts with what was seen when ALF adsorbs CO_2, where the strong hydrogen bonding between the small cavity formate hydrogens and the CO_2 oxygen atoms causes a contraction of the framework.[20] Further results from in situ X-ray monitoring are shown in Figure S4 in the Supporting Information, including how the B_{eq} (Debye–Waller factor) of the atoms of the ALF framework change upon O_2 adsorption. Of note, one may expect that the carbon B_{eq} would decrease if the formate C–H was engaging in strong hydrogen bonding with the adsorbed O_2 molecule in the small cavity. However, this does not appear to be the case. The hydrogen bonding interactions between the formate hydrogens and the O_2 molecules are relatively weak, having interaction lengths almost ≈0.5 Å longer than the distance seen between the formate hydrogen and oxygen atoms of CO_2 (O_2 O–O–H distances 2.82(9) and 2.99(9) Å compared to the CO_2 O–C–O–H distance of 2.42(1) Å).[20] Figure 2d illustrates how, when normalized for multiplicity, the large cavity within ALF adsorbs O_2 at a faster rate/quantity than the small cavity, which aligns with the density functional theory (DFT)-calculated heat of adsorption for the cavities, as described below. Note that hydrogen bonding is not possible between O_2 and the framework in the larger cavities because the C–H bonds of the formate ions point only to the small cavities. In view of these observations, we believe that the hydrogen bonding effect is not an important factor for O_2 adsorption within the pores of ALF. Given the kinetic effects present in ALF, we do not reach maximum O_2 adsorption for 1.45 bar O_2 at 195 K even after 240 min. However, when given enough time to reach equilibrium, as during the in situ neutron powder diffraction experiment shown in Figure 2a, the refined value of adsorbed O_2 at 250 K under 1.1 bar is 1.22(7) mmol/g, compared to the predicted isotherm value of 1.22 mmol/g (Figure S9). The neutron diffraction refinement lends much credence to our proposed structural model and provides confidence that our molecular positions and occupancies are accurate. Figure 2e,f shows how the O_2 molecule positions were modeled for the small cavity and large cavity, respectively.

Raman spectra collected simultaneously during the in situ synchrotron X-ray diffraction experiment monitored a large spectral range between 150 and 3850 cm^{-1}. Each scan was time-stamped to a corresponding X-ray diffraction pattern. Figure 3a–c, which cumulatively displays the range 150–3200

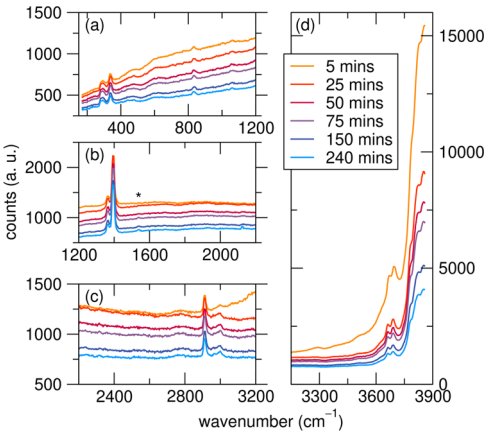

Figure 3. Raw Raman data (collected with a 532 nm laser) taken during the in situ O_2 gas dosing synchrotron X-ray diffraction experiments at 190 K, 1.45 bar O_2 [APS, 17-BM]. (a) Spectral range between 150 and 1200 cm^{-1}. (b) Spectral range between 1200 and 2200 cm^{-1}. (c) Spectral range between 2200 and 3200 cm^{-1}. (d) Spectral range between 3100 and 3850 cm^{-1}.

cm^{-1}, shows that there is no appreciable change in most of the observed peaks. However, one noticeable point of interest is the growth of the oxygen Raman signal near 1550 cm^{-1} (Figure 3b, denoted with a *), which grows more intense as the oxygen concentration increases in ALF.[18] In addition, Figure 3d displays the range between 3200 and 3850 cm^{-1}. This spectral range is usually ascribed to hydroxyl or amino N/O–H stretching frequencies. However, in ALF, the peaks observed here are not water or other species, as they do not match well-known frequencies which span over the entire range of 3000–3600 cm^{-1},[22] and the material was thoroughly activated prior to O_2 dosing. Instead, these peaks are from a sub percent Cr^{3+} contaminant present in the sample (the ALF sample tested is actually $Al_{0.996}Cr_{0.004}(HCOO)_3$; inductively coupled plasma (ICP) results are in the Supporting Information) and are anti-Stokes sidebands of the strong field fluorescence of the Cr^{3+} atoms. We confirm the existence of this fluorescence with accurate photoluminescence measurements, as shown in Figure S6. This minor contaminant was surprising and appeared to have been carried over from an undisclosed impurity in a purchased precursor. Regardless, this impurity proves to be serendipitously useful in terms of monitoring oxygen adsorption. As the oxygen concentration increases, the fluorescence in the 3000 and 3850 cm^{-1} spectral range decreases in intensity, with the most dramatic signal decrease occurring after the first 25 min of exposure (coinciding with the immediate O_2 adsorption in ALF). This decrease in signal as a function of O_2 adsorption is due to the quenching of Cr^{3+} fluorescence by paramagnetic O_2.[23] Though the Cr^{3+} contaminant at this level was unintended and has no impact on the O_2 adsorption performance of the material, this level of Cr^{+3} doping may suggest a relevant synthetic choice for using ALF as a sensing material for O_2 adsorption.

First-principle density functional theory (DFT) calculations have also been performed to understand the O_2 adsorption mechanism in $Al(HCOO)_3$. The relative position energies of O_2 in the small and large cavities of ALF are shown in Figure 4.

https://doi.org/10.1021/jacs.3c02100
J. Am. Chem. Soc. XXXX, XXX, XXX–XXX

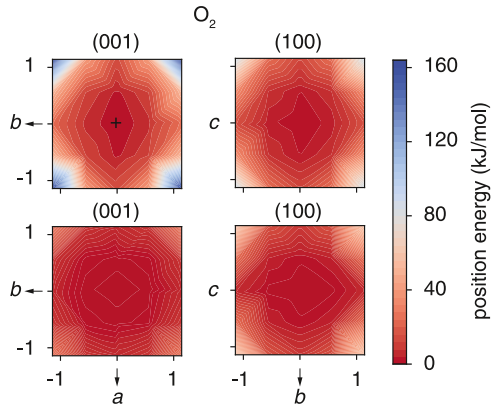

Figure 4. Relative position energies of O_2 within $Al(HCOO)_3$ in small (top) and large (bottom) cavities. The O_2 position energies at cavity centers are set as 0. Positive energies (blue) suggest energetically unfavorable locations.

The energy landscape of O_2 in ALF was probed as the molecule was moved in the two cavities. Two main trends can be observed: (1) the energy minima (red areas), which are indicative of a favorable interaction of O_2 molecules with ALF, are all located at the center of the cavities. (2) The energy landscape of the larger cavity (bottom panels of Figure 4) appears much flatter than the small cavity, which suggests that O_2 molecules can favorably adsorb in ALF over a larger volume of the cavity. The calculated adsorption energies for O_2 in the small (−23.97 kJ/mol per O_2) and large (−24.77 kJ/mol per O_2) cavities are similar, with a marginal difference of ≈0.8 kJ/mol per O_2. The predicted adsorption energies agree well with the measured heat of adsorption (Q_{st}) for O_2 in ALF (derived from isotherms), which is initially ≈−21.5 kJ/mol and drops to ≈−20.5 kJ/mol as O_2 loading increases (Figure S10).

The O_2 adsorption isotherms of ALF reveal an effective adsorption maximum at ≈200 K, which is atypical because most MOFs adsorb more gas as the temperature is decreased. However, similar behavior has been observed in other microporous systems. This atypical phenomenon is attributed to the fact that microporous materials have more subtle framework−gas interactions and has been seen in at least two well-known examples, namely, zeolite type-A[24] and a non-ReO_3-type Mn(II) formate material.[25] In the case of the Mn(II) formate, the authors postulated that the material has a "dynamic opening of the pore aperture and/or sufficient kinetic energy of the adsorbates to overcome a diffusion barrier above a critical temperature." We believe that there is a similar effect in ALF and that this effect is associated with the kinetics of passing through the small apertures between ALF's cavities. Indeed, we also observed it in our work on CO_2 adsorption in ALF,[20] and it seems likely that "critical gating temperatures" exist that are dependent on the identity of the sorbate. This critical gating temperature range, which likely follows a thermally activated statistical distribution, also contributes to the reduced O_2/N_2 selectivity observed as temperature increases above 200 K. With increased temperature, conditions exceed those that are optimal for O_2 adsorption per the heat of adsorption of O_2 (−21.5 kJ/mol). In addition, lattice expansion and increased dynamics of the ALF framework reduce discriminatory gating against N_2 (heat of adsorption in ALF ≈−28 kJ/mol).

Lastly, though the performance of ALF is excellent at temperatures cooler than ≈250 K, kinetic effects become more pronounced and hysteresis between adsorption and desorption increases (Figure S9). We discuss briefly here a chemical strategy for creating Fe-substituted solid solutions with ALF to increase initial O_2 adsorption. However, though we discuss Fe-substituted solid solutions in this present work, the principle of metal substitution within ALF applies to many viable 3+ metals, as appreciated by the doping of Cr(III) mentioned above. The intended goal with other metal-aluminum ALF solid solutions would be to adjust the pore gating within the structure with larger/smaller ions, given the considerations of the previous paragraph, altering adsorption as well as other physical properties (like fluorescence) of the material. In the present study, the material targeted was an Al/Fe compound with a nominal 25:75 ratio, but from Rietveld refinement (Figure S3) and energy-dispersive X-ray (EDX) measurements (Figure S19), the material is, in fact, closer to an Al/Fe ratio of 40:60. We call this compound ALF-Fe. Interestingly, ALF-Fe shows markedly similar behavior to ALF in terms of absolute adsorption behavior (Figures S17 and S18) but with the advantage of having approximately 3-fold faster O_2 adsorption (Figures S14−S18). As explained in Figures S7 and S8, this is not a particle size effect, as ALF-Fe has a larger particle size as deduced from Brunauer−Emmett−Teller (BET) and pore-volume analysis done with N_2 at 77 K. As shown in Figure S5, the structure of ALF-Fe has a lowered symmetry (space group 195 instead of 204 for ALF) and has two metal sites alongside two symmetrically distinct formate ligands. The two metal sites are distinguished with one site being purely Fe and the other being 80/20 Al/Fe. The metal−oxygen distances within the pure Fe octahedra are 1.96(5) and 1.98(3) Å, compared with 1.83(3) and 1.86(6) Å for the mixed Fe/Al octahedra. The lower symmetry of ALF-Fe relative to ALF was established due to additional Bragg reflections in the powder pattern that can be indexed through subgroup relationships to space group 195. In effect, ALF-Fe is the first example of a doubled ReO_3-type formate.[21]

The faster O_2 adsorption with ALF-Fe relative to ALF at all temperatures is exciting and we believe it to be caused by channels in the material that have less pronounced formate hydrogen gating between cavities (Figure S5). However, given the reduced formate hydrogen gating between cavities, we would also expect that ALF-Fe would have different O_2/N_2 selectivity—which it does. As can be seen from Figure S18, O_2/N_2 selectivity with ALF-Fe drops consistently faster than ALF at our examined temperatures/air pressure conditions, although it shows up to 4-fold higher initial selectivity at 200 K. At 200 K, the very rapid O_2 adsorption in ALF-Fe engenders an O_2/N_2 selectivity between 400 and 100 for the first minute, dropping to ≈50 after 5 min. At temperatures above 200 K, ALF-Fe displays O_2/N_2 selectivity beneath 10. Considering that these selectivity results are approximations derived from single component isotherms, the O_2/N_2 selectivity using a multicomponent mixture is likely higher, particularly at 200 K, given the fast and substantial O_2 adsorption. In general, ALF-Fe and related congeners would likely lend themselves to rapid temperature swing processes for O_2 separation if properly tuned. We believe that further examination of the numerous metal solid solutions within the ALF family will likely lead to useful behavior in several gas separations/gas adsorptions.

https://doi.org/10.1021/jacs.3c02100
J. Am. Chem. Soc. XXXX, XXX, XXX−XXX

CONCLUSIONS

A combination of adsorption, diffraction, spectroscopic, and computational investigations have given a detailed insight into the selective adsorption of O_2 from air into aluminum formate (ALF). We have also demonstrated that metal substitution in the ALF family is a viable tool for tuning the selectivity and kinetics of the system. We wish to emphasize how ALF differs from most prior MOF studies where open metal sites play crucial roles in the selective binding of O_2.[26,27] It appears that the excellent O_2/N_2 separation performance in ALF is due to molecular sieving that takes advantage of the small difference between the kinetic diameters of O_2 and N_2. Our findings show that pore-size engineering in MOFs is a powerful tool for designing new materials for air separation. To the best of our knowledge, ALF has the highest O_2/N_2 sorption selectivity verified by co-adsorption experiments among MOF adsorbents without open metal sites.[9] With its great application potential for noncryogenic air separation demonstrated, ALF also has a significant advantage compared with all other MOFs in terms of its ease of synthesis, low cost, and scalability.[20]

ASSOCIATED CONTENT

Supporting Information

The Supporting Information is available free of charge at https://pubs.acs.org/doi/10.1021/jacs.3c02100.

Description of experimental materials and methods, additional figures on PXRD analysis and gas adsorption measurements on ALF and ALF-Fe, photoluminescence, SEM of different ALF particle size samples, and tables on computationally derived parameters for ALF (PDF)

Accession Codes

CCDC 2218471−2218473 contain the supplementary crystallographic data for this paper. These data can be obtained free of charge via www.ccdc.cam.ac.uk/data_request/cif, or by emailing data_request@ccdc.cam.ac.uk, or by contacting The Cambridge Crystallographic Data Centre, 12 Union Road, Cambridge CB2 1EZ, UK; fax: +44 1223 336033.

AUTHOR INFORMATION

Corresponding Authors

Hayden A. Evans − *Center for Neutron Research, National Institute of Standards and Technology, Gaithersburg, Maryland 20899, United States;* orcid.org/0000-0002-1331-4274; Email: hayden.evans@nist.gov

Dan Zhao − *Department of Chemical and Biomolecular Engineering, National University of Singapore, 117585, Singapore;* orcid.org/0000-0002-4427-2150; Email: chezhao@nus.edu.sg

Pieremanuele Canepa − *Department of Materials Science and Engineering, National University of Singapore, 117575, Singapore; Department of Chemical and Biomolecular Engineering, National University of Singapore, 117585, Singapore;* orcid.org/0000-0002-5168-9253; Email: pcanepa@nus.edu.sg

Anthony K. Cheetham − *Department of Materials Science and Engineering, National University of Singapore, 117575, Singapore; Materials Research Laboratory, University of California, Santa Barbara, Santa Barbara, California 93106, United States;* orcid.org/0000-0003-1518-4845; Email: akc30@cam.ac.uk

Authors

Dinesh Mullangi − *Department of Materials Science and Engineering, National University of Singapore, 117575, Singapore*

Taner Yildirim − *Center for Neutron Research, National Institute of Standards and Technology, Gaithersburg, Maryland 20899, United States*

Yuxiang Wang − *Department of Chemical and Biomolecular Engineering, National University of Singapore, 117585, Singapore*

Zeyu Deng − *Department of Materials Science and Engineering, National University of Singapore, 117575, Singapore;* orcid.org/0000-0003-0109-9367

Zhaoqiang Zhang − *Department of Chemical and Biomolecular Engineering, National University of Singapore, 117585, Singapore;* orcid.org/0000-0002-9172-2871

Thuc T. Mai − *Physical Measurement Laboratory, National Institute of Standards and Technology, Gaithersburg, Maryland 20899, United States*

Fengxia Wei − *Institute of Materials Research and Engineering, Agency for Science Technology and Research, 138634, Singapore;* orcid.org/0000-0002-2058-5056

John Wang − *Department of Materials Science and Engineering, National University of Singapore, 117575, Singapore;* orcid.org/0000-0001-6059-8962

Angela R. Hight Walker − *Physical Measurement Laboratory, National Institute of Standards and Technology, Gaithersburg, Maryland 20899, United States;* orcid.org/0000-0003-1385-0672

Craig M. Brown − *Center for Neutron Research, National Institute of Standards and Technology, Gaithersburg, Maryland 20899, United States; Department of Chemical and Biomolecular Engineering, University of Delaware, Newark, Delaware 19716, United States;* orcid.org/0000-0002-9637-9355

Complete contact information is available at: https://pubs.acs.org/10.1021/jacs.3c02100

Author Contributions

○D.M. and H.A.E. contributed equally to this work.

Notes

The authors declare the following competing financial interest(s): A patent has been filed by the National University of Singapore and Agency for Science Technology and Research based on the present results (SG Non-Provisional Application No. 10202106057Y).

The authors declare the following competing financial interest(s): A patent has been filed by the National University of Singapore and the Agency for Science Technology and Research based on the present results (SG Non-Provisional Application No. 10202106057Y). All data needed to evaluate the conclusions in the paper are present in the paper and/or the Supporting Information.

ACKNOWLEDGMENTS

This work was partially supported by the following: the National Research Council of the United States of America for financial support through the Research Associate Program (H.A.E.), the NIST Center for Neutron Research (H.A.E., C.M.B.), the Singapore Ministry of Education Academic Fund Tier 1 (Grants R-284-000-186-133 and R-284-000-194-114) (P.C., Z.D.), the Singapore MOE-Academic Research Fund

(R-284-000-193-114) (D.M., A.K.C., J.W.), the Singapore Ministry of Education (Tier 1, A8000186-01-00, J.W.), the National Research Foundation under the fellowship NRFF12-2020-0012 (P.C.), the National University of Singapore Green Energy Programme for funding under the project code R-284-000-185-731 (A.K.C., D.Z., J.W., P.C.), funding from the Lee Kuan Yew Postdoctoral Fellowship (Grant No. 22-5930-A0001) (Z.D.), the Agency for Science, Technology and Research (U2102d2004) (Y.W., Z.Z., D.Z.), and the Ras al Khaimah Centre for Advanced Materials (A.K.C.). The computational work was performed on resources of the National Supercomputing Centre, Singapore (https://www.nscc.sg/). Powder X-ray diffraction data were collected on beamline 17-BM at the Advanced Photon Source at the Argonne National Laboratory, which is supported by the U.S. Department of Energy, Office of Science, Office of Basic Energy Sciences under contract DEAC02-06CH11357. Neutron diffraction data were collected on BT-1 at the NIST Center For Neutron Research, and we acknowledge the support of the National Institute of Standards and Technology, U.S. Department of Commerce, in providing the neutron research facilities used in this work. Certain commercial equipment, instruments, or materials are identified in this document. Such identification does not imply recommendation or endorsement by the National Institute of Standards and Technology, nor does it imply that the products identified are necessarily the best available for the purpose.

REFERENCES

(1) Francis, R.; Byrne, G. Duplex Stainless Steels—Alloys for the 21st Century. *Metals* **2021**, *11*, No. 836.
(2) Jha, M.; Gaur, N. Life Cycle of Medical Oxygen from Production to Consumption. *J. Family Med. Prim. Care.* **2022**, *11*, 1231−1236.
(3) Castle, W. F. Air Separation and Liquefaction: Recent Developments and Prospects for the Beginning of the New Millennium. *Int. J. Refrig.* **2002**, *25*, 158−172.
(4) Smith, L. J.; Eckert, H.; Cheetham, A. K. Site Preferences in the Mixed Cation Zeolite, Li, Na-Chabazite: A Combined Solid-State NMR and Neutron Diffraction Study. *J. Am. Chem. Soc.* **2000**, *122*, 1700−1708.
(5) Koh, D.-Y.; Pimentel, B. R.; Babu, V. P.; Stephenson, N.; Chai, S. W.; Rosinski, A.; Lively, R. P. Sub-Ambient Air Separation via Li^+ Exchanged Zeolite. *Microporous Mesoporous Mater.* **2018**, *256*, 140−146.
(6) Shaban, H. I. A Study of Foaming and Carry-Over Problems in Oil and Gas Separators. *Gas Sep. Purif. Technol.* **1995**, *9*, 81−86.
(7) Chong, K. C.; Lai, S. O.; Thiam, H. S.; Teoh, H. C.; Heng, S. L. Recent Progress of Oxygen/Nitrogen Separation Using Membrane Technology. *J. Eng. Sci. Technol.* **2016**, *11*, 1016−1030.
(8) Bi, X.; Meng, X.; Liu, P.; Yang, N.; Zhu, Z.; Ran, R.; Liu, S. A Novel CO_2-Resistant Ceramic Dual-Phase Hollow Fiber Membrane for Oxygen Separation. *J. Membr. Sci.* **2017**, *522*, 91−99.
(9) Sutton, A. L.; Melag, L.; Sadiq, M. M.; Hill, M. R. Capture, Storage, and Release of Oxygen by Metal−Organic Frameworks (MOFs). *Angew. Chem., Int. Ed.* **2022**, *61*, No. e202208305.
(10) Reed, D. A.; Xiao, D. J.; Jiang, H. Z.; Chakarawet, K.; Oktawiec, J.; Long, J. R. Biomimetic O_2 Adsorption in an Iron Metal−Organic Framework for Air Separation. *Chem. Sci.* **2020**, *11*, 1698−1702.
(11) Shimomura, S.; Higuchi, M.; Matsuda, R.; Yoneda, K.; Hijikata, Y.; Kubota, Y.; Mita, Y.; Kim, J.; Takata, M.; Kitagawa, S. Selective Sorption of Oxygen and Nitric Oxide by an Electron-Donating Flexible Porous Coordination Polymer. *Nat. Chem.* **2010**, *2*, 633−637.
(12) Ma, S.; Wang, X. S.; Collier, C. D.; Manis, E. S.; Zhou, H. C. Ultramicroporous Metal−Organic Framework Based on 9,10-Anthracenedicarboxylate for Selective Gas Adsorption. *Inorg. Chem.* **2007**, *46*, 8499−8501.
(13) Ma, S.; Wang, X. S.; Yuan, D.; Zhou, H. C. A Coordinatively Linked, Doubly Interpenetrated, Yb Metal-Organic Framework Demonstrates High Thermal Stability and Uncommon Gas-Adsorption Selectivity. *Angew. Chem., Int. Ed.* **2008**, *47*, 4130−4133.
(14) DeCoste, J. B.; Weston, M. H.; Fuller, P. E.; Tovar, T. M.; Peterson, G. W.; LeVan, M. D.; Farha, O. K. Metal-Organic Frameworks for Oxygen Storage. *Angew. Chem., Int. Ed.* **2014**, *53*, 14092−14095.
(15) Alezi, D.; Belmabkhout, Y.; Suyetin, M.; Bhatt, P. M.; Weseliński, L. J.; Solovyeva, V.; Adil, K.; Spanopoulos, I.; Trikalitis, P. N.; Emwas, A. H.; Eddaoudi, M. MOF Crystal Chemistry Paving the Way to Gas Storage Needs: Aluminum-Based soc-MOF for CH_4, O_2, and CO_2 Storage. *J. Am. Chem. Soc.* **2015**, *137*, 13308−13318.
(16) Chao, C. C. Process for Separating Nitrogen from Mixtures Thereof with Less Polar Substances. US4,859,217, Aug 22, 1989.
(17) Bloch, E. D.; Murray, L. J.; Queen, W. L.; Chavan, S.; Maximoff, S. N.; Bigi, J. P.; Krishna, R.; Peterson, V. K.; Grandjean, F.; Long, G. J.; Smit, B.; et al. Selective Binding of O_2 Over N_2 in a Redox−Active Metal−Organic Framework with Open Iron(II) Coordination Sites. *J. Am. Chem. Soc.* **2011**, *133*, 14814−14822.
(18) Xiao, D. J.; Gonzalez, M. I.; Darago, L. E.; Vogiatzis, K. D.; Haldoupis, E.; Gagliardi, L.; Long, J. R. Selective, Tunable O_2 Binding in Cobalt (II)−Triazolate/Pyrazolate Metal−Organic Frameworks. *J. Am. Chem. Soc.* **2016**, *138*, 7161−7170.
(19) Murray, L. J.; Dinca, M.; Yano, J.; Chavan, S.; Bordiga, S.; Brown, C. M.; Long, J. R. Highly-Selective and Reversible O_2 Binding in Cr_3(1,3,5-benzenetricarboxylate)$_2$. *J. Am. Chem. Soc.* **2010**, *132*, 7856−7857.
(20) Evans, H. A.; Mullangi, D.; Deng, Z.; Wang, Y.; Peh, S. B.; Wei, F.; Wang, J.; Brown, C. M.; Zhao, D.; Canepa, P.; Cheetham, A. K. Aluminum Formate, $Al(HCOO)_3$: An Earth-Abundant, Scalable, and Highly Selective Material for CO_2 Capture. *Sci. Adv.* **2022**, *8*, No. eade1473.
(21) Evans, H. A.; Wu, Y.; Seshadri, R.; Cheetham, A. K. Perovskite-Related ReO_3-Type Structures. *Nat. Rev. Mater.* **2020**, *5*, 196−213.
(22) Carey, D. M.; Korenowski, G. M. Measurement of the Raman Spectrum of Liquid Water. *J. Chem. Phys.* **1998**, *108*, 2669−2675.
(23) Oter, O.; Ribou, A. C. Quenching of Long Lifetime Emitting Fluorophores with Paramagnetic Molecules. *J. Fluoresc.* **2009**, *19*, 389−397.
(24) Breck, D. W.; Eversole, W. G.; Milton, R. M.; Reed, T. B.; Thomas, T. L. Crystalline Zeolites. I. The Properties of a New Synthetic Zeolite, Type A. *J. Am. Chem. Soc.* **1956**, *78*, 5963−5972.
(25) Kim, H.; Samsonenko, D. G.; Yoon, M.; Yoon, J. W.; Hwang, Y. K.; Chang, J. S.; Kim, K. Temperature-Triggered Gate Opening for Gas Adsorption in Microporous Manganese Formate. *Chem. Commun.* **2008**, *39*, 4697−4699.
(26) Jaramillo, D. E.; Jaffe, A.; Snyder, B. E.; Smith, A.; Taw, E.; Rohde, R. C.; Dods, M. N.; DeSnoo, W.; Meihaus, K. R.; Harris, T. D.; Neaton, J. B.; Long, J. R. Metal−Organic Frameworks as O_2-Selective Adsorbents for Air Separations. *Chem. Sci.* **2022**, *13*, 10216−10237.
(27) Demir, H.; Stoneburner, S. J.; Jeong, W.; Ray, D.; Zhang, X.; Farha, O. K.; Cramer, C. J.; Siepmann, J. I.; Gagliardi, L. Metal−Organic Frameworks with Metal−Catecholates for O_2/N_2 Separation. *J. Phys. Chem. C* **2019**, *123*, 12935−12946.

https://doi.org/10.1021/jacs.3c02100
J. Am. Chem. Soc. XXXX, XXX, XXX−XXX